Microwave Underground Propagation and Detection

Lawrence Carin, *Fellow, IEEE*, Jeffrey Sichina, and James F. Harvey, *Senior Member, IEEE*

Invited Paper

***Abstract*—The detection of buried targets has been a problem of significant interest for decades, with microwave-based sensing constituting an important tool. In this paper, we review the basic issues that characterize microwave-based subsurface sensing. Issues considered include the use of microwaves in the context of an airborne synthetic aperture radar, as well for radars deployed close to the air–soil interface. Rough-surface induced clutter is also discussed. Particular examples are presented for detection of land mines and unexploded ordnance.**

***Index Terms*—Ground penetrating radar, synthetic aperture radar, ultra-wide-band.**

I. Introduction

UNDERGROUND sensing is of interest in many applications, including detection of buried conduits, minerals, chemicals and possibly ordnance. Due to high attenuation in most soils, microwave-based underground sensing is most appropriate for targets on or near the air–soil interface. In this paper, we attempt to cover the general area of radar-based subsurface sensing, with particular examples presented for sensing surface and subsurface land mines and unexploded ordnance (UXO).

For both the UXO and land-mine problems, there is often the need to perform quick wide-area surveillance, to circumscribe regions likely to contain mine fields or former bombing ranges. In such a problem, one is *not* interested in detecting *each* individual mine or UXO, rather the presence of a high-enough concentration of such to warrant deployment of ground-based sensors (such as induction sensors [1]). In practice, a former bombing range is typically littered with UXO and/or other man-made debris that is near or on the soil interface. Since minimal soil penetration is required for such missions, microwave systems constitute a viable technology. Similar issues hold for detection of a mine field.

While the UXO and land-mine problems constitute particular examples, the issues found in sensing such targets are of interest for a wide range of microwave-based subsurface sensing problems.

Manuscript received October 21, 2001.

L. Carin is with the Department of Electrical and Computer Engineering, Duke University, Durham, NC 27708-0291 USA.

J. Sichina is with the Army Research Laboratory, AMSRL-SE-RU, Adelphi, MD 20783 USA.

J. F. Harvey is with the Army Research Office, Research Triangle Park, NC 27709-2211 USA.

Publisher Item Identifier S 0018-9480(02)01961-0.

II. Modeling Underground Propagation and Scattering

A. Method of Moments (MoM)

The MoM constitutes a widely employed tool for general scattering problems. A MoM analysis typically employs a background-medium Green's function; with this, often a layered medium in the context of subsurface sensing. For the land-mine problem, the analysis may be even further simplified since many land mines are rotationally symmetric [a body of revolution (BoR)]. If the BoR axis of rotation is perpendicular to the surfaces of the layered medium, one can analyze the scattering via a so-called two-and-one-half dimensional (2.5-D) MoM analysis [2], [3].

The principal challenge in development of a MoM model for targets in layered media, *vis-à-vis* a free-space MoM analysis, involves evaluation of the dyadic layered-medium Green's function [4], each component of which is expressed in terms of an oscillatory Sommerfeld integral. For scattering problems at radar frequencies, we have found the complex-image technique [5] to be a particularly accurate and efficient means of analyzing such integrals. In this approach, the spectral-domain reflection coefficient is represented via a finite exponential expansion, using a technique such as Prony's method [6].

B. Fast-Multipole Methods

Assume that N basis functions are used for representation of the currents on the target. A MoM analysis of such a scattering problem requires order N^2 memory, order N^2 CPU time to fill the matrix, and order N^3 or $P \cdot N^2$ CPU time for matrix solution (for an LUD or iterative matrix solution [7], respectively, where P represents the number of iterations required for convergence). For the triangle-patch basis functions typically utilized [8], one generally requires 7–10 basis functions per wavelength. This implies that, as the target becomes large electrically (frequency increases), the number of basis functions N can become large, restricting either the target size that can be considered at a given frequency or the upper frequency at which a particular target can be analyzed. The MoM model has, therefore, recently been extended to the fast multipole method (FMM) [9]–[11].

The FMM realizes an efficient means of computing the N^2 interactions between expansion and testing functions. In particular, the expansion and testing functions are segmented into a set of clusters, and the interactions are computed between the clusters, rather than between the individual expansion and testing functions. The fundamental identity that underpins the FMM

requires that the clusters be "far enough" apart [9]–[11], with this typically slightly larger than a cluster diameter. Therefore, the "far" interactions are computed via the FMM cluster–cluster methodology, and the relatively few interactions not so evaluated are computed as in the traditional MoM. These latter components are called the "near" terms. In the FMM, the cluster sizes are fixed, while further acceleration can be achieved by using multilevel cluster sizing, in a tree-like procedure [11]. In this approach, we first consider large-sized clusters, and compute all cluster–cluster interactions allowed by the FMM identity. Each cluster is then divided into eight smaller clusters, and all interactions not accounted for at the parent level are performed at the smaller (children) cluster level, for all such interactions permitted by the FMM identity. This multilevel fast multipole algorithm (MLFMA) can achieve order $N \log N$ memory requirements and a $P \cdot N \log N$ CPU requirement [11].

The original FMM and MLFMA were developed for targets in free space [9]–[11] since the fundamental FMM identities are based on the free-space Green's function. The FMM and MLFMA have recently been extended to the case of general conducting or dielectric target in the presence of a half-space or layered medium [12]–[15]. The steepest descent path method has further accelerated the FMM for shallow targets [16].

C. Finite-Difference Methods

The MoM, FMM, and MLFMA algorithms are very powerful tools, but they are limited to relatively regular structures. In particular, as discussed above, such methods employ a background Green's function [2]–[4], often in the form of a layered medium [2]–[4]. While general inhomogeneities can be placed in the vicinity of such a background medium, it is often preferable to employ a more general formalism from the outset. In this context, there has been significant interest in the finite difference time domain (FDTD) [17]–[19] and, more recently, in the multiresolution time domain (MRTD) [20]. The FDTD typically expands the fields in terms of pulse basis functions, in both space and time [17]–[19]. The MRTD expands the fields more generally in terms of a wavelet basis [20], this often yielding improved numerical properties. The FDTD and MRTD have been applied to a wide range of subsurface-sensing problems, in which, for example, the complete antenna structure has been modeled rigorously [17]–[19].

III. Synthetic Aperture Radar (SAR)

A. Example Measurement System

SAR plays an important role in wide-area subsurface sensing. We present SAR imagery for an example system. In particular, the Army Research Laboratory, Adelphi, MD, has developed an experimental ultra-wide-band (UWB) SAR system. The system has been deployed at the Yuma Proving Ground, Yuma, AZ, to test microwave sensing of surface and buried land mines and UXO. The UWB SAR system is operated directly in the time domain, covering a usable bandwidth of approximately 50–1200 MHz. The pulse emitted by the radar, as well as other details of the sensor, is discussed in [21] and [22].

B. SAR Image Formation

The SAR is moved along a straight path and, for each position, the scattered response is measured. In its simplest embodiment, the bipolar image amplitude I_{mn} at pixel position (m, n) is given by

$$I_{mn} = \sum_{k=1}^{Ks} s_k(t = T_{k,m,n}) \tag{1}$$

where $s_k(t)$ represents the time-domain scattered field measured at the kth sensor position and $T_{k,m,n}$ is the round-trip time delay between sensor position k and the physical position in the image represented by pixel (m, n).

Equation (1) gives the connection between the measured (time-domain) fields and the subsequent SAR image. For a comparison of theoretical and measured SAR imagery, it is essential to use (in the theory) an incident waveform consistent with that of the actual UWB SAR system. It should be noted, however, that, in general, the antennas have frequency-dependent properties that have a strong angular dependence [22]. Moreover, each of the waveforms $s_k(t)$ measured along the SAR aperture constitutes a different angle between the sensor and target. Therefore, in actuality, there is *not* a single pulse shape incident on the target from all aperture positions. Similar issues hold with regard to the polarization purity—an antenna may be vertically polarized at boresight, but the polarization can change markedly with angle. To account for this, only a limited number of aperture positions are used to image a given pixel in the SAR image (such that the properties of the incident field on that pixel are similar for all waveforms used in image formation).

C. Measured Versus Modeled: Land Mines

We consider the M20 antitank mine, a relatively large conducting target, shown in Fig. 1. The measured and computed (bipolar) SAR imagery are compared in Fig. 2 for the M20 mine flush buried just under the surface, for VV polarization (vertical incident polarization, vertical received polarization). From these results, we see that the agreement between the measured and computed imagery is good, but the background clutter corrupts the measured signal.

In Fig. 2, we have concentrated on a large conducting antitank mine, with the motivation that such are likely to be the easiest targets to detect with an airborne system. However, many land mines are nearly entirely plastic and relatively small, and it is of interest to quantify the difficulty of radar-based detection of such *vis-a-vis* large metal targets such as the M20 considered in Fig. 2.

We consider UWB plane-wave scattering from a "PMN2" plastic antipersonnel (AP) mine (inset in Fig. 3), with the incident waveform discussed above. The mine is characterized by a dielectric constant $\varepsilon_r = 2.9 - j0.01$. The results in Fig. 3 present the time-domain scattered fields from the PMN2 AP mine buried to a depth of 2 cm in Yuma soil (see [22]), considering 0%, 5%, 10%, 15%, and 20% water by weight and an incidence angle of $\theta_i = 60^\circ$ with respect to the normal. As a comparison, scattering results are also shown for the M20 mine

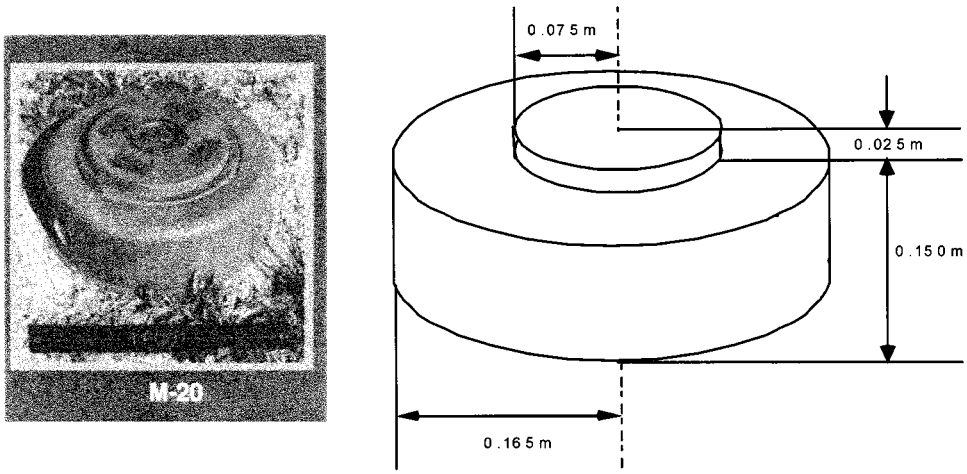

Fig. 1. M20 antitank mine used in measurements and calculations.

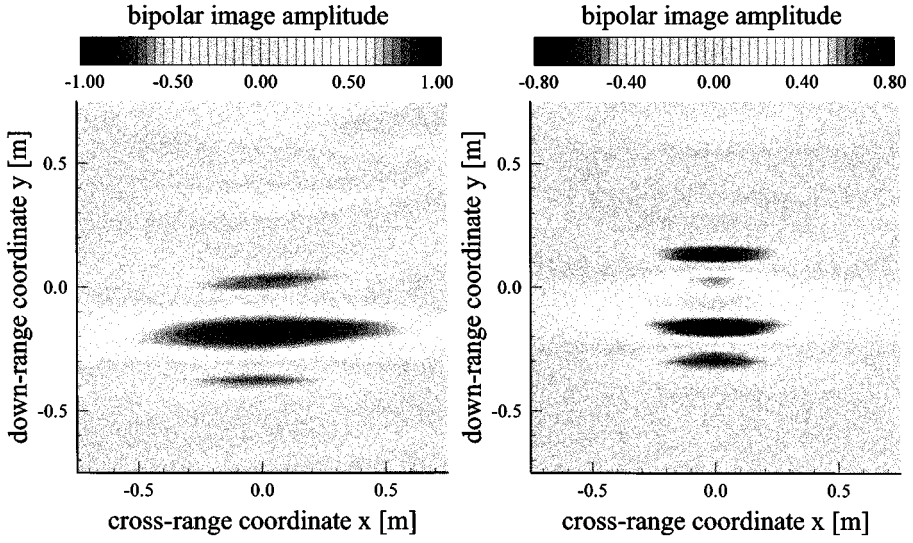

(a) (b)

Fig. 2. Comparison of: (a) measured and (b) computed SAR images for mine in Fig. 1 situated in the Yuma soil [22]. The mine is flush buried just under the surface.

buried 15.24 cm. We see in Fig. 3, for VV polarization, that the waveform scattered from the mine in 5% soil is dramatically smaller than that of the buried M20 mine. Similar results hold for HH polarization.

The results in Fig. 3 demonstrate that the increased water content dramatically increases the signatures of plastic AP mines, with this phenomenon aided in large measure by the fact that AP mines are usually buried at quite shallow depths. The increased water content enhances the electrical contrast between the background soil and plastic target.

D. Measured Versus Modeled: UXO

Example data is presented for the 155 mm shell shown in Fig. 4 for the test site at the Yuma Proving Ground. For these measurements, the Yuma soil was characterized by approximately 5% water content, with the associated electrical properties described in [22]. All measured results are for the UXO buried just under the air–ground interface, with the target axis parallel to the interface (flush buried). The gridded model of the target, used in the numerical computations, is shown in Fig. 5.

In Fig. 5, the shell axis is oriented 45° to the linear SAR aperture. For all images, the total angle spanned by the linear aperture relative to the target center is 60°° The agreement between the model and measured SAR image is reasonable, especially considering the complexity of the experimental system and the uncertainty in the angle-dependent incident-wave polarization and pulse shape. When tilted at 45°, the scattered return is characterized by two diagonally offset returns, characteristic of diffraction from the target front and back. Note that, in the model results in Fig. 5, one can almost distinguish the two (diagonally offset) scattering mechanisms, while in the measured response these appear to merge into a single diagonal response. This may be due to an over estimation in the model of the SAR's cross-range resolution. Moreover, random motion of the sensor, for example, due to wind, also undermines the resolution of the measured image.

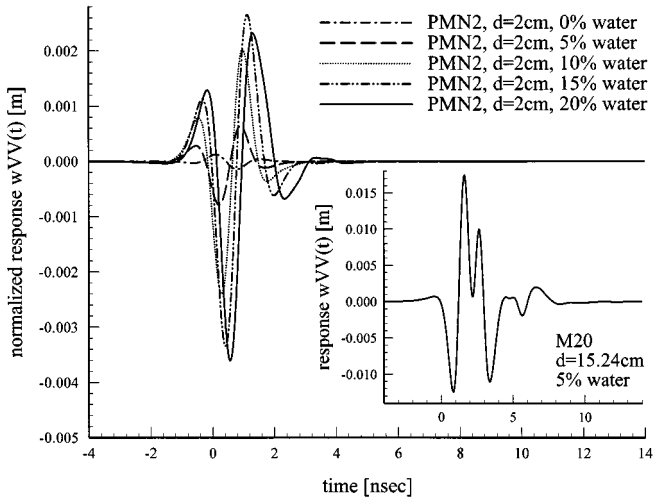

Fig. 3. UWB plane-wave scattering from a "PMN2" plastic mine (inset in Fig. 3). The mine is buried at a depth of 2 cm in Yuma soil [22], considering 0%, 5%, 10%, 15%, and 20% water by weight and an incidence angle of $\theta_i = 60°$. As a comparison, scattering results are also shown for the 15.24-cm-deep M20 mine (5% water content). Results are shown for VV polarization.

Fig. 4. Photograph of a 155-mm shell.

While the theoretical SAR image in Fig. 5 captures most of the features in their measured counterparts, we notice several features in the measured images that are not seen in the computed data. The image features not modeled by the theory are attributed to clutter, this constituting one of the principal challenges to SAR-based sensing. The measurements were taken in a relatively benign environment, with minimal foliage cover on the flat terrain. Consequently, the clutter in Fig. 5 is attributed primarily to subsurface soil inhomogeneities.

IV. Rough Air–Soil Interface

A. Fractal Surface

Natural scenes often manifest a multiscale structure that cannot be described by only one parameter (e.g., a correlation length). The recently developed fractal framework [24] has proven a good approach for describing a multitude of natural phenomena, including natural rough interfaces. Recent papers have studied the scattering of electromagnetic waves from fractal surfaces, using analytical as well as numerical methods [26]–[28]. Theoretically, random fractal surface models take into account the roughness over an infinite range of scales. However, fractal surfaces cannot be handled rigorously in practice because of their peculiar mathematical properties, among which are nonstationarity and the consequent inappropriateness of defining a power spectrum. For practical purposes, we, therefore, must restrict ourselves to the study of band-limited fractals [26].

As an example, in the following, we consider the band-limited Weierstrass process [26], [29]:

$$w(x) = \sigma \sqrt{\frac{2(1-b^{-2H})}{b^{-2HN_1} - b^{-2H(N_2+1)}}} \times \sum_{n=-N_1}^{N_2} b^{-Hn} \cos(2\pi b^n x + \varphi_n) \quad (2)$$

where σ is the standard deviation, H is the Hurst exponent with values between 0–1, $b > 1$ is a constant (we take $b = \sqrt{\pi}$), and φ_n are random phases, uniformly distributed between 0–2π. The fractal dimension of this process is $D = 2 - H$. It can be shown that the spectrum of a Weierstrass process follows a power law (*i.e.*, $S(k) \propto k^{-2H-1}$) [26], [29].

B. Truncating the Surface

In any numerical model of rough-surface scattering, the surface must be finite, making edge effects an important issue. One solution to this problem is to consider illumination by a beam [24], [30]–[33]. This is often employed as the incident field in frequency-domain integral-equation solvers [30]–[33]. However, the beam approach is difficult to implement with time-domain methods, if one tries to model wide-band electromagnetic scattering. This is because the beamwidth increases with the wavelength, which means that for the low frequencies of the spectrum we need an impractically large computational domain. We consider scattering from a finite-extent surface, under pulsed *plane-wave* excitation, with the surface constituting a discontinuity in an infinite half-space background [34]. As mentioned, the plane-wave excitation gives rise to edge effects at the ends of the finite rough surface. The received time sequence is windowed temporally, with the scattered-field statistics computed by considering only a portion of the transient signature in the middle of the time-domain response, this weakly affected by edge diffraction (in the beam approach, the beamwidth windows the problem spatially). The MRTD model considered here employs a finite two-dimensional rough surface in the vicinity of an *infinite* dielectric half-space [34]. The diffracted fields from the ends of the rough surface are, therefore, generated by the relatively smooth transition from a half-space to a rough surface. Moreover, the rough surface is tapered at the ends to avoid sharp peaks in the vicinity of the terminal points.

C. Example Results

The large number of rough-surface calculations (600 rough-surface calculations are used to obtain the statistics below) requires an efficient implementation of the MRTD algorithm [34]. The soil is modeled as a lossy dielectric, with $\varepsilon_r = 6$ and $\sigma = 0.005$ S/m, independent of frequency. These parameters are typical for dry soil. A more realistic soil model should account for a variation of these parameters with frequency (i.e., dispersion).

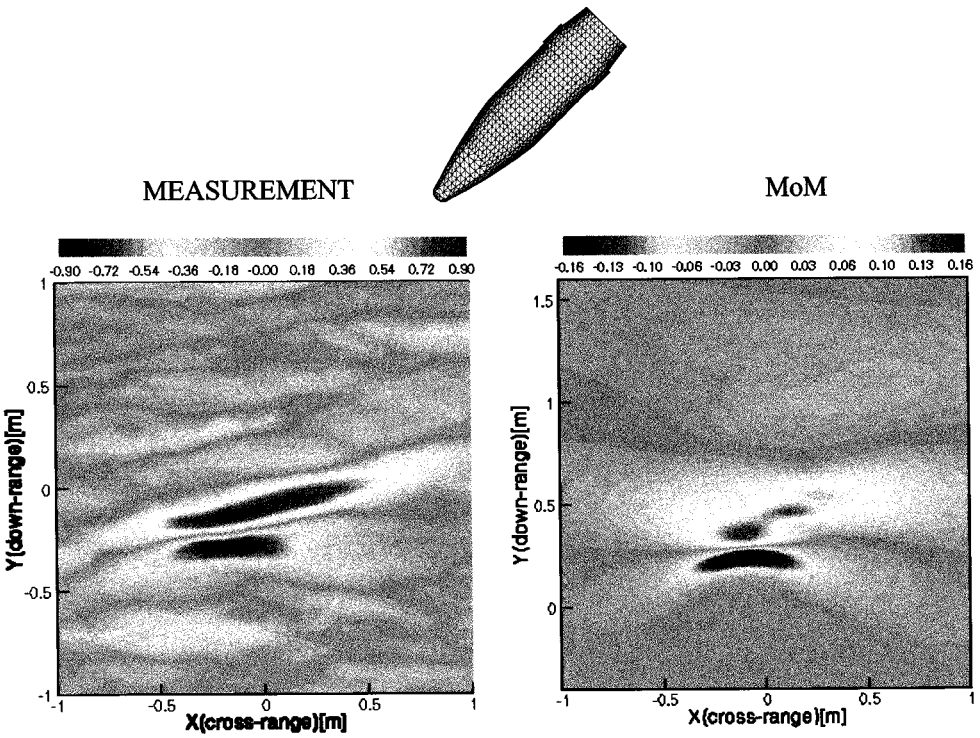

Fig. 5. Comparison of computed and measured SAR images for the 155-mm shell (Fig. 4) flush buried in 5% Yuma soil [22]. The computations use pulsed plane-wave excitation at 30° from grazing. The measured and computed images use an aperture length that yields a 60° angle between the target center and aperture. The shell axis is oriented 45° from the linear SAR aperture.

The incident field is implemented as a pulsed plane wave, radiating in the presence of an infinite planar half-space. The rough surface induces perturbations to this incident wave, yielding the scattered fields. The incident time-domain waveform is a Rayleigh fourth-order pulse [35], and its central frequency (300 MHz) is also characteristic of applications involving subsurface sensing [21]. Here, we employ a Haar-based MRTD scheme with one level of wavelets. The MRTD discretization rate is 40 Haar scaling functions per central wavelength in air, which implies about six Haar scaling functions per wavelength at the smallest wavelength in the spectrum, in the denser medium (when wavelets are considered as well, this corresponds to 12 cells per smallest wavelength in terms of equivalent Yee cells). The observations are always made in backscatter, at a distance of $1000\lambda_c$ (far zone) from the target, where λ_c is the central wavelength of the pulse in air.

Of interest is the length of the rough surface employed in the computations. As indicated above, the rough surface is modeled as a finite-length perturbation to an infinite half-space. The onset of the rough surface is smoothed such that diffraction at the edge of the rough surface is minimized. For the cases studied here, we have found that a surface length of approximately $12.5\lambda_c$ is normally sufficient (where λ_c is the central wavelength of the incident pulse), even at incidence angles of 65° with respect to the normal. Numerical details on this issue can be found in [36].

In Fig. 6, we plot the estimated power spectral density (PSD) of the surface-induced backscattered clutter for a Weierstrass fractal surfaces, for incidence 25° from grazing, for both TE and TM polarization (all results are two-dimensional). The central wavelength of the incident pulse is $\lambda_c = 1$ m. The fractal surfaces are characterized by the standard deviation $\sigma = 6.25$ cm and fractal dimension $D = 1.5$. Other important parameters of the Weierstrass fractal surfaces are the order of the lowest and highest harmonics N_1 and N_2. For fractal dimension $D = 1.2$, $N_1 = 2$ and $N_2 = 12$, while for fractal dimension, $D = 1.5$, $N_1 = 2$, and $N_2 = 15$. It is important to note that the clutter strength for TM polarization is larger than that for TE. This issue plays an important role in choosing the appropriate polarization for target detection [34].

The Weierstrass fractal surfaces described in (2) is characterized by the superposition of harmonics with random phase. Each harmonic corresponds to a finite periodic surface and, therefore, diffraction from each is characterized by scattering in terms of a set of Floquet modes [37]. Each Floquet mode propagates at a frequency-dependent angle, with the angle of propagation representative of the backscattered direction at particular frequencies. This yields the fractal-surface induced clutter in Fig. 6, in which particular Floquet modes yield a strong backscatter response at particular frequencies. The number of Floquet modes excited is dependent on the excitation incidence angle, increasing as one gets closer to grazing.

V. Downward-Looking Microwave Systems

Synthetic-aperture radar plays an important role in wide-area sensing for subsurface targets such as mines and UXO. After identifying a region in which such targets may be located, it is of interest to deploy systems that are closely coupled to the ground. This is also true for sensing other targets, such as buried conduits. As an example, in Fig. 7, we depict a horn antenna, with

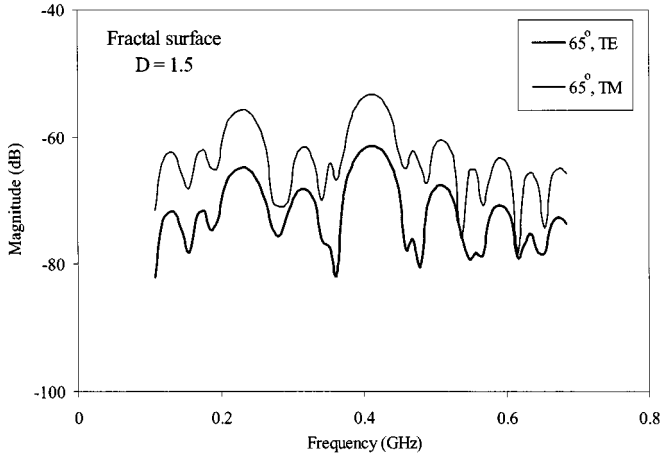

Fig. 6. Power spectrum density of backscattered fields, scattered by a fractal surface with $\sigma = 6.25$ cm and $D = 1.5$ for incidence 65° from the normal.

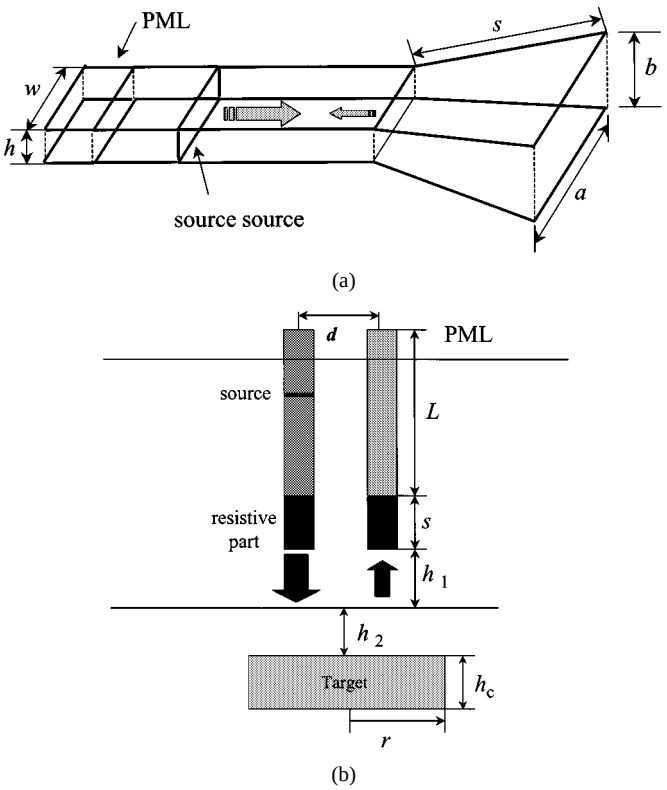

Fig. 7. Antenna used in ground-penetrating radar study. (a) Details of the transmitting antenna. (b) Dual-antenna bistatic system.

the horn composed of a tapered resistive material, to minimize artifacts introduced by the antenna and by soil–antenna interaction [17]–[19]. Such antennas are detailed in [19].

As an example of the type of data one can obtain from such an antenna system, in Fig. 8, we present a comparison of measured and computed data, with the computations performed via MRTD. The measurements were performed at the U.S. Army Night Vision and Electronic Sensors Directorate (NVESD) test facility (Ft. Belvoir, VA), in which the soil under test is approximately homogeneous to a significant depth, with which systems can be studied in a well-characterized environment (providing a good test of the model).

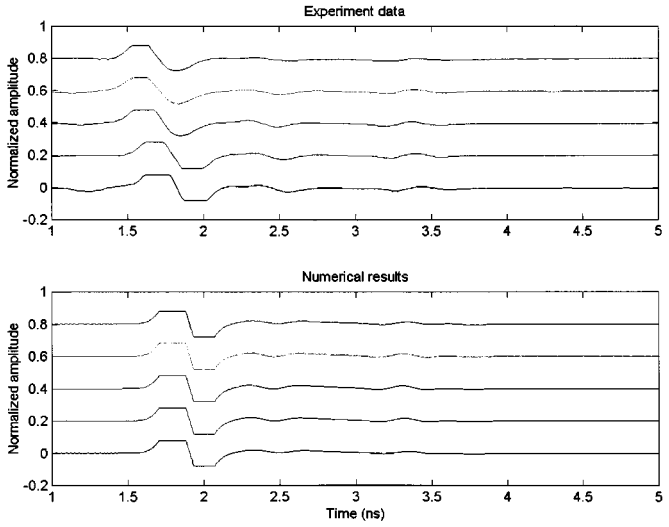

Fig. 8. Comparison of computed (bottom) and measured (top) transient fields for five positions of the dual-antenna system relative to the target. The results correspond to a buried dielectric cylinder of dimensions $h_1 = 11$ cm, $h_2 = 5$ cm, $h_c = 7.5$ cm, and $r = 7.5$ cm [see Fig. 7(b)]. The background soil is characterized by $\varepsilon_r = 2.5$ and $\sigma = 0.005$ S/m, and the lossless dielectric-cylinder target is characterized by $\varepsilon_r = 3.0$.

Measurements were performed to characterize the electrical properties of the soil used in the measurements (here, highly sandy soil), approximately characterized by $\varepsilon_r = 2.5$ and $\sigma = 0.005$ S/m (there was very little dispersion; the test facility is indoors and, therefore, the soil water content is essentially zero). The target under consideration is an approximately lossless dielectric cylinder of 15-cm diameter and 7.5-cm height, with the top of the cylinder parallel to the flat air–soil interface at a depth of 5 cm. The dielectric constant of the cylinder is $\varepsilon_r = 3.0$, constituting a very weak target-soil contrast. The end of the horns was 11 cm from the air–soil interface, with the plates of the parallel-plate waveguides oriented perpendicular to the interface.

Five curves are presented in Fig. 8, representing different positions of the two antennas relative to the buried dielectric target (with the sensor at a fixed height); two adjacent antennas of the form in Fig. 7 constitute the radar system, one antenna for transmission and the other for reception. The middle curve corresponds to the axis of the cylinder positioned at the midpoint of the two antennas, with the other results corresponding to shifts of the entire antenna system by increments of 5 cm. For example, the top curves corresponds to a shift to one side by 10 cm, and the bottom curve represents a shift to the other side, again, by 10 cm. The remaining two curves address similar issues, now for a 5-cm offset.

The first strong response in each curve corresponds to reflection at the air–soil interface, with the two subsequent waveforms corresponding to reflection at the top and bottom of the dielectric target. We have clipped the initial response such that the target signature is visible (this underscores the weakness of the target response). While there are differences between the measured and computed data, it is clear from Fig. 8 that the model results capture the principal scattering physics seen in the measured data.

The amplitudes of the computed results in Fig. 8 are normalized as follows. We compute the peak radiated field E_p,

as measured just before the fields hit the air–soil interface. For the case of a buried target, the amplitude of the computed scattered fields are normalized to E_P. The reflection coefficient for a plane wave incident normally upon the soil considered in Fig. 5 is $\Gamma = 0.225$. The peak value of the initial scattered waveform in Fig. 8 has a relative amplitude just below Γ (not shown explicitly in Fig. 8, due to the clipping). Alternative applications for radar-based near-soil sensing are discussed in [38] and [39].

VI. Other Applications of Microwaves in Subsurface Sensing

We have presented examples of microwaves employed in the context of SAR and for a downward-looking radar. For the former, the sensor is typically distant from the targets of interest, while in the latter, the antenna is often in close contact with the soil. In Section IV, we discussed clutter issues introduced by rough-surface scattering.

It is of interest to note other applications microwaves have been applied toward, in the context of subsurface sensing. As an alternative to electromagnetic waves, researchers have directed significant attention toward employing acoustic or elastic waves to sense buried targets. One of the difficulties of such sensors is that acoustic/elastic waves often decay quickly in soil. This significantly complicates sensing, if one requires the acoustic/elastic waves to interact with a target of interest, and then propagate back to the acoustic/elastic sensor. To eliminate the required return path of the acoustic/elastic waves from the target back to the sensor, investigators have employed microwaves. In particular, microwaves are used to sense the small surface acoustic vibrations, these introducing a Doppler shift to the microwaves [40], [41]. This yields a hybrid acoustic–microwave sensor, synergistically exploiting the strengths of both sensor modalities.

VII. Summary

This paper has attempted to summarize some of the issues of interest in microwave (radar) sensing of targets in the vicinity of soil. Land mines and UXO have been a principal focus of this discussion, although radar-based subsurface sensing is also of interest in such areas as detection of buried conduits. Clutter constitutes a significant limitation of microwave-based subsurface sensing and, in this context, we have also addressed scattering from a statistically rough soil interface. We have demonstrated that microwaves play a role in wide-area subsurface sensing (i.e., SAR), as well as for localized near-ground sensing.

References

[1] L. Carin, H. T. Yu, Y. Dalichaouch, and C. Baum, "On the wideband EMI response of a rotationally symmetric permeable and conducting target," *IEEE Trans. Geosci. Remote Sensing*, vol. 39, pp. 1206–1213, June 2001.

[2] S. Vitebskiy, K. Sturgess, and L. Carin, "Short-pulse plane-wave scattering from buried perfectly conducting bodies of revolution," *IEEE Trans. Antennas Propagat.*, vol. 44, pp. 143–151, Feb. 1996.

[3] N. Geng and L. Carin, "Wideband electromagnetic scattering form a dielectric BOR buried in a layered, dispersive medium," *IEEE Trans. Antennas Propagat.*, vol. 47, pp. 610–619, Apr. 1999.

[4] K. A. Michalski and D. Zheng, "Electromagnetic scattering and radiation by surfaces of arbitrary shape in layered media: Parts I and II," *IEEE Trans. Antennas Propagat.*, vol. 38, pp. 335–352, Mar. 1990.

[5] R. M. Shubair and Y. L. Chow, "A simple and accurate complex image interpretation of vertical antennas present in contiguous dielectric half-spaces," *IEEE Trans. Antennas Propagat.*, vol. 41, pp. 806–812, June 1993.

[6] M. L. Van Blaricum and R. Mittra, "A technique for extracting the poles and residues of a system directly from its transient response," *IEEE Trans. Antennas Propagat.*, vol. AP-23, pp. 777–781, Nov. 1975.

[7] G. H. Golub and C. F. van Loan, *Matrix Computations*. Baltimore, MD: The Johns Hopkins Univ., 1996.

[8] S. M. Rao, D. R. Wilton, and A. W. Glisson, "Electromagnetic scattering from surfaces of arbitrary shape," *IEEE Trans. Antennas Propagat.*, vol. AP-30, pp. 409–418, May 1982.

[9] R. Coifman, V. Rokhlin, and S. Wandzura, "The fast multipole method for the wave equation: A pedestrian prescription," *IEEE Trans. Antennas Propagat. Mag.*, vol. 35, pp. 7–12, June 1993.

[10] J. M. Song and W. C. Chew, "Fast multipole method solution using parametric geometry," *Microwave Opt. Technol. Lett.*, vol. 7, pp. 760–765, Nov. 1994.

[11] J. M. Song, C. C. Lu, and W. C. Chew, "Multilevel fast multipole algorithm for electromagnetic scattering by large complex objects," *IEEE Trans. Antennas Propagat.*, vol. 45, pp. 1488–1493, Oct. 1997.

[12] N. Geng, A. Sullivan, and L. Carin, "Fast multipole method for scattering from an arbitrary PEC target above or buried in a lossy half space," *IEEE Trans. Antennas Propagat.*, vol. 49, pp. 740–748, May 2001.

[13] ——, "Multilevel fast-multipole algorithm for scattering from conducting targets above or embedded in a lossy half space," *IEEE Trans. Geosci. Remote Sensing*, vol. 38, pp. 1561–1573, July 2000.

[14] J. Q. He, A. Sullivan, and L. Carin, "Multilevel fast multipole algorithm for three-dimensional dielectric targets in the vicinity of a lossy half space," *Microwave Opt. Technol. Lett.*, vol. 29, pp. 100–104, Apr. 2001.

[15] B. Hu and W. C. Chew, "Fast inhomogeneous plane wave algorithm for scattering from objects above the multilayered medium," *IEEE Trans. Geosci. Remote Sensing*, vol. 39, pp. 1028–1038, May 2001.

[16] M. El-Shenawee, C. Rappaport, E. L. Miller, and M. B. Silevitch, "Three-dimensional subsurface analysis of electromagnetic scattering from penetrable/PEC objects buried under rough surfaces: Use of the steepest descent fast multipole method," *IEEE Trans. Geosci. Remote Sensing*, vol. 39, pp. 1174–1182, June 2001.

[17] J. M. Bourgeois and G. S. Smith, "A fully three-dimensional simulation of ground penetrating radar: FDTD theory compared with experiment," *IEEE Trans. Geosci. Remote Sensing*, vol. 34, pp. 28–36, Jan. 1996.

[18] G. S. Smith and L. E. R. Petersson, "On the use of evanescent electromagnetic waves in the detection and identification of objects buried in lossy soil," *IEEE Trans. Antennas Propagat.*, vol. 48, pp. 1295–1300, Sept. 2000.

[19] T. P. Montoya and G. S. Smith, "Land mine detection using a ground-penetrating radar based on resistively loaded Vee dipoles," *IEEE Trans. Antennas Propagat.*, vol. 47, pp. 1795–1806, Dec. 1999.

[20] X. Zhu and L. Carin, "Multi-resolution time-domain analysis of scattering from general dielectric targets in the presence of a half space," *IEEE Trans. Antennas Propagat.*, vol. 49, pp. 1568–1578, Nov. 2001.

[21] M. A. Ressler and J. W. McCorkle, "Evolution of the army research laboratory ultra-wideband test bed," in *Ultra-Wideband Short-Pulse Electromagnetics 2*, L. Carin and L. B. Felsen, Eds. New York: Plenum, 1995, pp. 109–123.

[22] L. Carin, N. Geng, M. McClure, J. Sichina, and L. Nguyen, "Ultra-wide-band synthetic-aperture radar for mine-field detection," *IEEE Antennas Propagat. Mag.*, vol. 41, pp. 18–33, Feb. 1999.

[23] T. Dogaru and L. Carin, "Time-domain sensing of targets buried under a Gaussian, exponential, or fractal rough interface," *IEEE Trans. Geosci. Remote Sensing*, vol. 39, pp. 1807–1819, Aug. 2001.

[24] F. D. Hastings, J. B. Schneider, and S. L. Broschat, "A Monte Carlo FDTD technique for rough surface scattering," *IEEE Trans. Antennas Propagat.*, vol. 43, pp. 1183–1191, Nov. 1995.

[25] B. B. Mandelbrot, *The Fractal Geometry of Nature*. New York: Freeman, 1983.

[26] D. L. Jaggard and Y. Kim, "Diffraction by band-limited fractal screens," *J. Opt. Soc. Amer. A, Opt. Image Sci.*, vol. 4, pp. 1055–1062, June 1987.

[27] S. Rouvier, P. Borderies, and I. Chenerie, "Ultra-wideband electromagnetic scattering of a fractal profile," *Radio Sci.*, vol. 32, no. 2, pp. 285–293, Mar.–Apr. 1997.

[28] E. Bachelier, C. Ruiz, P. Borderies, I. Chenerie, and M. Davidson, "Weierstrass functions determination for soil modeling," in *Proc. Geosci. Remote Sensing Symp.*, vol. 3, Seattle, WA, 1998, pp. 1207–1209.

[29] M. V. Berry and Z. V. Lewis, "On the Weierstrass–Mandelbrot fractal function," in *Proc. R. Soc. Lond. A, Math. Phys. Sci.*, 1980, pp. 459–484.
[30] M. Saillard and D. Maystre, "Scattering from metallic and dielectric rough surfaces," *J. Opt. Soc. Amer. A, Opt. Image Sci.*, vol. 7, pp. 982–990, June 1990.
[31] E. I. Thorsos, "The validity of the Kirchoff approximation for rough surface scattering using a Gaussian roughness spectrum," *J. Acoust. Soc. Amer.*, vol. 83, pp. 78–92, 1988.
[32] E. I. Thorsos and D. R. Jackson, "The validity of the perturbation approximation for rough surface scattering using a Gaussian roughness spectrum," *J. Acoust. Soc. Amer.*, vol. 86, pp. 261–277, 1989.
[33] J. T. Johnson and R. J. Burkholder, "Coupled canonical grid/discrete dipole approach for computing scattering from objects above or below a rough interface," *IEEE Trans. Geosci. Remote Sensing*, vol. 39, pp. 1214–1220, June 2001.
[34] T. Dogaru and L. Carin, "Time-domain sensing of targets buried under a Gaussian, exponential, or fractal rough interface," *IEEE Trans. Geosci. Remote Sensing*, vol. 39, pp. 1807–1819, Aug. 2001.
[35] P. Hubral and M. Tygel, "Analysis of the Rayleigh pulse," *Geophysics*, vol. 54, pp. 654–658, 1989.
[36] T. Dogaru, "Modeling and Signal Processing for Electromagnetic Subsurface Sensing," Ph.D. dissertation, Elect. Comput. Eng. Dept., Duke Univ., Durham, NC, 1999.
[37] D. L. Jaggard and Y. Kim, "Diffraction by band-limited fractal screens," *J. Opt. Soc. Amer. A, Opt. Phys. Image Sci.*, vol. 4, pp. 1055–1062, June 1987.
[38] C.-C. Chen, M. B. Higgins, K. O'Neill, and R. Detsch, "Ultrawide-bandwidth fully-polarimetric ground penetrating radar classification of subsurface unexploded ordnance," *IEEE Trans. Geosci. Remote Sensing*, vol. 39, pp. 1221–1230, June 2001.
[39] B. Yang and C. Rappaport, "Response of realistic soil for GPR applications with 2-D FDTD," *IEEE Trans. Geosci. Remote Sensing*, vol. 39, pp. 1198–1205, June 2001.
[40] W. R. Scott, J. S. Martin, and G. D. Larson, "Experimental model for a seismic landmine detection system," *IEEE Trans. Geosci. Remote Sensing*, vol. 39, pp. 1155–1164, June 2001.
[41] C. T. Schroder and W. R. Scott, "A finite-difference model to study the elastic-wave interactions with buried land mines," *IEEE Trans. Geosci. Remote Sensing*, vol. 38, pp. 1505–1512, July 2000.

Lawrence Carin (S'85–M'85–SM'96–F'01) was born on March 25, 1963 in Washington, DC. He received the B.S., M.S., and Ph.D. degrees in electrical engineering from the University of Maryland at College Park, in 1985, 1986, and 1989, respectively.

In 1989, he joined the Electrical Engineering Department, Polytechnic Institute of New York, Brooklyn, NY, as an Assistant Professor, and became an Associate Professor in 1994. In September 1995, he joined the Electrical Engineering Department, Duke University, Durham, NC, where he is currently a Professor. He is the Principal Investigator on a multidisciplinary university research initiative (MURI) on demining. His current research interests include short-pulse scattering, subsurface sensing, and wave-based signal processing.

Dr. Carin is a member of Tau Beta Pi and Eta Kappa Nu. He is an associate editor of the IEEE TRANSACTIONS ON ANTENNAS AND PROPAGATION.

Jeffrey Sichina received the B.S.E.E. degree from the University of Pittsburgh, Pittsburgh, PA, in 1975. He subsequently began graduate study at the University of Maryland at College Park.

In 1974, he joined Harry Diamond Laboratories, Adelphi, MD. From 1974 to 1985, he was a Staff Engineer involved with a variety of electronic fuzing programs. His primary research interests have included digital signal processing, FM/CW systems, and electronic counter–counter measures. In 1986, he became a Project Officer for the Chaparral Air Defense System Target Detection Device Product Improvement Program. In 1988, he joined the Radar Branch, and was responsible for development of a miniature moving-target-indicator radar for unmanned air vehicles. In 1972, he became Chief of the Radar Branch, and was responsible for a variety of long-term applied research undertakings within the U.S. Army. Among these was an effort aimed at determining the effectiveness of UWB radar for detection of concealed objects, such as buried mines. His current research interest include algorithm development and detection theory.

Mr. Sichina is a member Eta Kappa Nu.

James F. Harvey (M'91–SM'99) received the B.S. degree in engineering from the U.S. Military Academy, West Point, NY, in 1964, the M.A. degree in physics from Dartmouth College, Hanover, NH, in 1972, and the Ph.D. degree in applied science from the University of California at Davis, in 1990, with research performed at the Lawrence Livermore National Laboratory.

He has served in a variety of electrical engineering and research assignments as a member of the U.S. military prior to retiring. He is currently a Civilian Research Program Manager at the Army Research Office, Research Triangle Park, NC, with primary responsibility within the fields of electromagnetics, antennas and antenna structures, innovative microwave and millimeter-wave circuit integration, low-power/minimum-power system design, and landmine detection. His programs include a focus on small, multifrequency, and multifunctional antennas for Army vehicles, radio propagation over complex terrain affecting data communications, new millimeter-wave circuit integration techniques such as spatial power combining, micromachining, and advanced electromagnetic calculational techniques. His personal research interests are in the fields of quasi-optics, radio-wave propagation, and multiresolution analysis of electromagnetic structures.

Dr. Harvey is an active member of the IEEE Microwave Theory and Techniques Society (IEEE MTT-S), the IEEE Antennas and Propagation Society (IEEE AP-S), URSI Commission D, and The International Society for Optical Engineers (SPIE). He is an organizer of the annual conference on the "Detection and Remediation Technologies for Mines and Minelike Targets" in the SPIE Aerosense Meeting and he is an editor of the conference proceedings. He was the recipient of the 1992 U.S. Army Research and Development Award.